Available online at website: https://journal.bcrec.id/index.php/bcrec

Bulletin of Chemical Reaction Engineering & Catalysis, 20 (2) 2025, 254-263

Original Research Article

Effect of Ammonia, Urea, and Magnesium Modification on γ-Al_2O_3 Support in Enhancing the Catalytic Performance for Hydrodemetallization and Hydrodesulfurization

Wawan Rustyawan[1], I.G.B.N Makertihartha[1,2], Oki Muraza[5], Ismal Gamar[5], Nadya Nurdini[3], Grandprix T.M. Kadja[2,3,4,*], Carolus B. Rasrenda[1,2,*]

[1]Department of Chemical Enginering, Institut Teknologi Bandung, Jl. Ganesha No. 10, Bandung 40132, Indonesia.
[2]Center for Catalysis and Reaction Engineering, Institut Teknologi Bandung, Jl. Ganesha no. 10, Bandung 40132, Indonesia.
[3]Division of Inorganic and Physical Chemistry, Faculty of Mathematics and Natural Sciences, Institut Teknologi Bandung, Jl. Ganesha no. 10, Bandung 40132, Indonesia.
[4]Research Center for Nanosciences and Nanotechnology, Institut Teknologi Bandung, Jl. Ganesha no. 10, Bandung 40132, Indonesia.
[5]Pertamina Technology & Innovation, Jl. Raya Bekasi KM. 20 Pulogadung, East Jakarta, Indonesia.

Received: 25th February 2025; Revised: 19th March 2025; Accepted: 20th March 2025
Available online: 21th March 2025; Published regularly: August 2025

Abstract

This research investigates the modification of γ−Al_2O_3 using ammonia, urea, and magnesium acetate to enhance its catalytic properties for hydrodemetallization (HDM) and hydrodesulfurization (HDS). Structural modifications affected the mineral composition, crystal size distribution, and textural properties of the support, with boehmite crystal sizes consistently ranging from 7 to 10 nm. Textural analysis indicated that alumina supports modified with urea and ammonia demonstrated enhanced characteristics, including elevated specific surface area (S_{BET}), pore volume (V_T), and pore size distribution (d), which are essential for catalytic performance. The modified catalyst (HM) exhibited significant hydrodemetalation efficiency, attaining metal removal rates of 98% for iron, 71% for vanadium, and 99% for nickel. In the HDS reaction, HM demonstrated the highest sulfur conversion of 20.9% at 315 °C, due to its capacity to sustain active site availability. The primary cause of catalyst deactivation was metal deposition, which resulted in pore blockage and diminished efficiency. The findings underscore the importance of support modification in enhancing catalytic performance, indicating HM as a viable catalyst for future heavy oil refining applications.

Keywords: Hydrodesulfurization (HDS); Hydrodemetallization (HDM); Fe (Iron) removal; Vanadium removal; Nickel removal

How to Cite: Rustyawan, W., Makertihartha, I. G. B. N., Muraza, O., Gamar, I., Nurdini, N., Kadja, G. T., Rasrenda, C. B. (2025). Effect of Ammonia, Urea, and Magnesium Modification on γ-Al_2O_3 Support in Enhancing the Catalytic Performance for Hydrodemetallization and Hydrodesulfurization. *Bulletin of Chemical Reaction Engineering & Catalysis*, 20 (2), 254-263. (doi: 10.9767/bcrec.20360)

Permalink/DOI: https://doi.org/10.9767/bcrec.20360

1. Introduction

The increasing demand for oil-based energy, driven by technological and industrial advancements, has made the efficiency of petroleum refining processes crucial to ensuring a sustainable energy supply. One of the primary strategies in refining heavy oil is hydrotreating, which includes hydrodesulfurization (HDS) and hydrodemetallization (HDM) to improve fuel quality by removing sulfur and heavy metals [1,2]. HDS plays a key role in reducing sulfur content to minimize harmful emissions, while HDM is essential for eliminating heavy metals, such as vanadium (V), nickel (Ni), and iron (Fe), which can

* Corresponding Author.
Email: grandprix.thomryes@itb.ac.id (G.T.M. Kadja)
cbr@itb.ac.id (C.B. Rasrenda)

poison catalysts and reduce process efficiency [3,4].

The effectiveness of HDS and HDM processes is significantly influenced by the properties of the catalyst used. One of the most commonly used catalyst support materials in hydrotreating is γ-Al_2O_3, due to its high surface area, excellent thermal stability, and tunable pore structure. However, a major challenge in its application is catalyst deactivation caused by coke deposition and metal accumulation during HDM. The buildup of heavy metals in catalyst pores leads to clogging, reducing accessibility to active sites and decreasing catalytic activity [5]. Therefore, catalyst modification is necessary to enhance its stability and performance in HDS and HDM reactions.

One promising approach is base modification of catalysts using ammonia, urea, and magnesium to optimize the textural and acid-base properties of γ-Al_2O_3, thereby enhancing its catalytic activity in HDS and HDM. Basic modification aims to adjust the acid-base balance of the catalyst, which is crucial in improving interactions between heavy oil compounds and active catalytic sites during hydrogenation and cracking reactions.

Ammonia is a base compound that enhances HDS activity by reducing excessive Brønsted acidity, which can hinder catalyst performance. Previous research has shown that ammonia improves hydrodesulfurization activity in CoMo/ASA and NiMo/ASA catalysts by interacting with Brønsted hydroxyl groups on the amorphous silica-alumina (ASA) support [6]. In the case of γ-Al_2O_3, ammonia modification increases the number of Lewis basic sites, which contribute to the adsorption and activation of sulfur-containing molecules, thereby accelerating desulfurization reactions. Additionally, ammonia helps improve catalyst resistance to coke formation, extending its lifespan during hydrotreating processes.

Urea plays a significant role in the synthesis of γ-Al_2O_3 by enhancing surface area and pore uniformity through the homogeneous precipitation mechanism of aluminum salts [7]. Studies have demonstrated that urea enhances HDS activity in NiMoP/Al_2O_3 catalysts, particularly at a urea/Ni ratio of 2. It promotes the uniform dispersion of MoO_x species and prevents the formation of inactive phases such as $NiMoO_4$ and $Al_2(MoO_4)_3$, which can reduce catalytic activity [8]. Furthermore, urea improves the diffusion capacity of heavy oil substrates into the catalyst pores, enhancing the overall efficiency of HDS reactions.

The modification of γ-Al_2O_3 with magnesium is intended to reduce acidity while increasing basicity, which contributes to the formation of CoMoS active sites in the HDS reaction. Research has shown that magnesium addition helps balance the acid-base properties of the catalyst, regulating the equilibrium between hydrogenation and cracking during HDS. Moreover, magnesium prevents coke formation by suppressing the unwanted polymerization of aromatic compounds. Previous studies have reported that modifying Mo/Al_2O_3 with Mg enhances catalytic activity in hydrodesulfurization (HDS) and hydrodenitrogenation (HDN) through a more efficient hydrogenation mechanism while also prolonging catalyst lifespan by mitigating deactivation due to coking [9,10].

Prior research has shown that increasing the specific surface area (S_{BET}), pore volume (V_T), and pore size distribution (d) of modified γ-Al_2O_3 contributes to enhanced catalytic activity in HDS and HDM. Catalysts with larger pore sizes and more uniform distribution allow better accessibility of heavy oil molecules to active sites, improving sulfur and metal removal efficiency [11,12]. Additionally, optimizing the acid-base balance of the catalyst through basic modification has been proven to improve selectivity in hydrodesulfurization reactions while preventing the formation of carbonaceous deposits that can deactivate the catalyst [13].

Therefore, this study aims to develop an optimized γ-Al_2O_3-based catalyst for hydrodesulfurization (HDS) and hydrodemetallization (HDM) reactions by modifying it with ammonia, urea, and magnesium. The modification is designed to enhance textural properties, control acid-base balance, and improve the efficiency of sulfur and heavy metal removal from heavy oil. Various formulations and combinations of modification materials were explored to achieve an optimal catalyst that is expected to contribute to more efficient heavy oil refining processes in the future.

2. Materials and Methods

2.1 Materials

The reagents employed in this study include Aluminium nitrate nonahydrate, $Al(NO_3)_3.H_2O$, Urea ($CO(NH_2)_2$), ammonia (NH_3), nickel (II) nitrate hexahydrate ($NiNO_3.6H_2O$, Sigma Aldrich), citric acid ($C_6H_8O_7$), molybdenum (VI) oxide (MoO_3, Sigma Aldrich), and Magnesium acetate ($(CH_3COO)_2Mg$). All these materials were procured from Merck and utilized without additional purifications. The feedstock model for HDS paraffinic sulfur standard and HDM activity (V, Ni & Fe-Naphthenate) in n-C16 to n-C18 solvent was obtained from Pertamina.

2.2. Preparation of Support

γ-Al_2O_3 supports were prepared with various modifications using Ammonia (NH_3), Urea, and

Mg-acetate ($(CH_3COO)_2Mg$). The synthesis of γ-Al_2O_3 involved mixing $Al(NO_3)_3$ with 100 mL of deionized water. Subsequently, the solutions were modified into four types according to the formula provided in Table 1, with continuous stirring for 10 minutes to ensure homogeneity of all reagents. The resulting solution was then placed in a hydrothermal autoclave and heated in an oven at a temperature of 170 ℃ for 18 hours. The subsequent steps included separating the precipitate from the solution through filtration, then drying at a temperature of 120 ℃ for 3 hours.

2.3. Preparation of Catalyst

An aqueous solution containing 1 gram of citric acid was combined with 28 grams of MoO_3 powder. Ammonia solution (NH_4OH) and 24 grams of $Ni(NO_3)_2.6H_2O$ crystals were then added and stirred until a homogeneous mixture was achieved. The optimized γ-Al_2O_3 support was positioned in a container and impregnated with the solution until full absorption occurred. The impregnated material was subsequently molded and subjected to calcination at 450 °C for a duration of 3 hours.

2.4. Characterizations Method

Several analysis methods were conducted to evaluate the characteristics and activity of all γ-Al_2O_3 catalysts in Hydrodemetallization (HDM) reaction, including X-ray diffraction (XRD), N_2 adsorption, and Specific Surface Area: The Brunauer–Emmett–Teller specific surface area (S_{BET}); The Barrett-Joyner-Halenda (BJH) pore volume (PV); and average pore diameter (APD). XRD analysis was performed utilizing the Bruker D2 PHASER XE-T 2nd generation diffractometer employing Cu-Kα radiation. The measurement data were recorded within 2θ of 5-90 °. N_2 adsorption-desorption was measured at 77 K on a Micromeritics TriStar II Plus 3.01, USA. The Specific Surface Area (S_{BET}, PV, APD) measurements were conducted on outgassed powders at 300 ℃ using Micromeritics FlowPrep 060, USA (sample degas system).

2.5. Hydrodemetallization (Fe, V and Ni) Activity Evaluation

The activity of catalysts in hydrodemetallization (HDM) for the removal of Iron (Fe), Vanadium (V), and Nickel (Ni) was evaluated, referencing the study by previous researcher [11], utilizing a high-pressure trickle-bed reactor pilot plant designed by Vinci Technology in downflow configuration. The reactor consists of a stainless steel tube with an inner diameter of 17.5 mm and a length of 925 mm, featuring a fixed-bed catalyst portion (Figure 1). The feedstock, containing Fe, V, and Ni impurities, was delivered into the reactor using a high-precision Eldex 5970 pump at a liquid hourly space velocity (LHSV) of 1 h^{-1}. The process transpired at a constant pressure of 32 bar, with hydrogen supplied at a H_2/oil ratio of 250:1 NL/L to facilitate the elimination of metal contaminants. The temperature varied from 195 °C to 315 °C to assess its effect on catalytic performance.

To assess the metal removal efficiency, around 1 g of the oil sample was subjected to ashing in a muffle furnace at 550 °C for a duration of 12 hours. The ash was dissolved in 2 mL of nitric acid and 0.5 mL of hydrochloric acid, subsequently transferred to a 25 mL volumetric flask for comprehensive mixing. The solution from the volumetric flask was then introduced into the spectrometer to determine the Fe, V, and Ni contents.

Table 1. Composition of γ-Al_2O_3 support formulation

No	Sample Code	$Al(NO_3)_3$ (mmol)	NH_3 (mmol)	Urea (mmol)	$(CH_3COO)_2Mg$ (mmol)
1	γ-Al_2O_3-AM1	40	85	-	-
2	γ-Al_2O_3-AM2		114	-	-
3	γ-Al_2O_3-AM3		142	-	-
4	γ-Al_2O_3-UA1		50	85	-
5	γ-Al_2O_3-UA2		50	114	-
6	γ-Al_2O_3-UA3		50	142	-
7	γ-Al_2O_3-UM1		-	50	7
8	γ-Al_2O_3-UM2		-	50	14
9	γ-Al_2O_3-UM3		-	50	21
10	γ-Al_2O_3-UMA1		50	7	28
11	γ-Al_2O_3-UMA2		50	7	57
12	γ-Al_2O_3-UMA3		50	7	85

2.6. Hydrodesulfurization Activity Evaluation

The catalysts' hydrodesulfurization (HDS) activity was assessed under conditions analogous to those of the HDM test. One gram of catalyst was added to the reactor. The flow of N_2 and H_2 gases from the cylinder was initiated previously. The line and reactor experienced oxygen removal, and the catalyst was dried with a nitrogen gas flow. The activation of the catalyst was performed through a sulfidation process, which involved the introduction of H_2 gas and a dimethyl disulfide solution (DMDS) in naphtha, leading to the generation of H_2S gas that permeated the catalyst compartment. The DMDS or naphtha feed stream was subsequently stopped, and the hydrodesulfurization process was resumed. Feed was supplied at a liquid hourly space velocity of 1, under a pressure of 32 bar, and at temperatures of 195, 255, 285, and 315 °C. Sampling was conducted during the storage of the product in a bottle containing the liquid. The product is analyzed for sulfur content.

3. Results and Discussion

3.1 Catalyst Characterizations

All forms of the γ-Al_2O_3 support were synthesized through three distinct chemical modifications, namely NH_3 (AM), Urea-NH_3 (UA), Urea-$(CH_3COO)_2Mg$ (UM), and Urea-$(CH_3COO)_2Mg$- NH_3 (UMA) with the formulation are detailed in Table 1 [14–16]. The mineral composition of the catalysts was investigated using XRD, as illustrated in Figure 2. The 2θ values corresponding to each peak in the XRD pattern are presented in Table 2, along with their respective *hkl* representations. The XRD results indicate that all samples exhibit peaks characteristic of boehmite, as compared to the standard boehmite from the JCPDS card 01-083-2384 [17–19]. All samples exhibit boehmite peaks at 2θ: ±14° (020), ±28° (120), ±38° (031), and ±48° (051). Additional analysis reveals the presence of

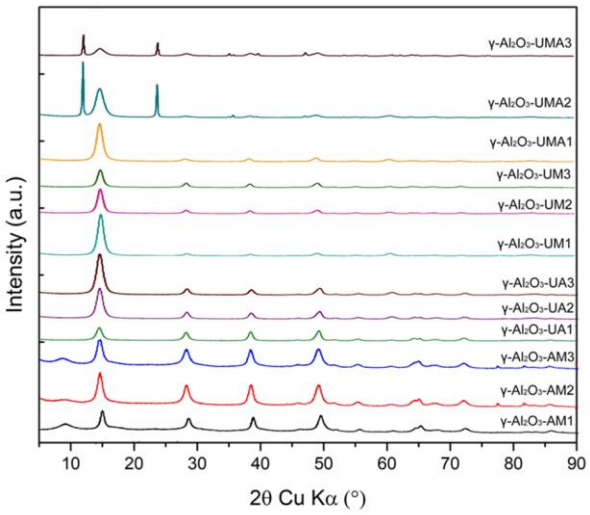

Figure 2. XRD pattern of γ-Al_2O_3 support using NH_3 (AM), Urea−NH_3 (UA), Urea−$(CH_3COO)_2Mg$ (UM), and Urea−$(CH_3COO)_2Mg$−NH_3 (UMA) as support variation.

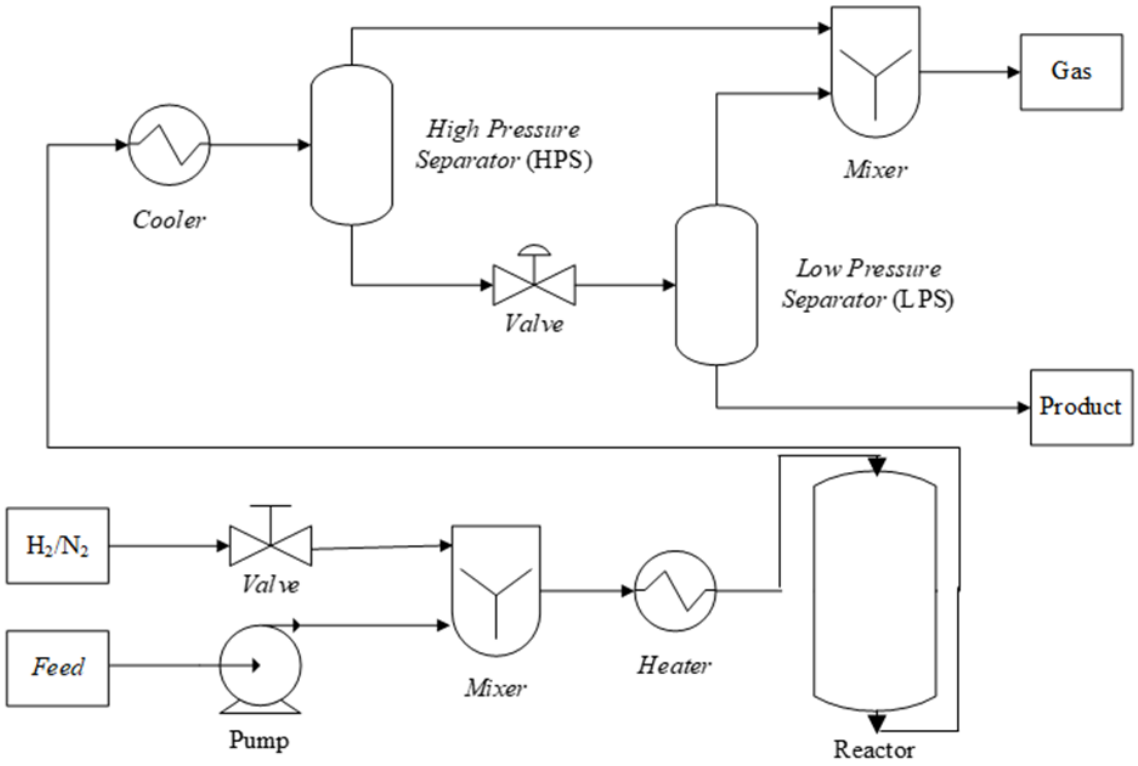

Figure 1. Schematic diagram of test equipment for NX1 hydroprocessing pilot plant reactor.

other crystals in the γ-Al_2O_3-UMA catalyst, indicated by supplementary peaks at ±12° and ±24°, likely corresponding to $Mg(OH)_2$ peaks originating from residual Mg acetate still present in the samples. This observation aligns with JCPDS file No. 00-044-1482 [20,21]. The presence of active metal phases, such as Ni and Mo, is confirmed by distinct diffraction peaks. The peaks at 2θ ≈ 37.2°, 43.3°, and 62.9° are attributed to NiO (JCPDS No. 47-1049), whereas the peaks at 2θ ≈ 12.8°, 23.3°, and 25.7° signify the presence of MoO_3 (JCPDS No. 35-0609). The diffraction peaks observed at 2θ ≈ 26.6° and 36.3° indicate the presence of $NiMoO_4$ (JCPDS No. 45-0142). Following the sulfidation process, the oxide phases are anticipated to transform into the active $NiMoS_2$ phase, which is identified by broad diffraction peaks at 2θ ≈ 14.4°, 33.5°, and 58.5° (JCPDS No. 37-1492). The lack of sharp peaks for $NiMoS_2$ indicates that the active phase is extensively dispersed on the catalyst support, which benefits catalytic performance.

Further analysis of the XRD pattern enables the determination of crystallite size using the Scherrer Equation based on the peak conditions of the XRD pattern. All samples exhibit relatively broad peaks, and according to the Scherrer Equation, the peak width is inversely proportional to the crystallite size [22–24]. Therefore, the calculated crystallite sizes for all samples are presented in Table 3. The crystallite size of the γ-Al_2O_3 support using NH_3 (AM), Urea-NH_3 (UA), Urea-$(CH_3COO)_2Mg$ (UM), and Urea-$(CH_3COO)_2Mg$-NH_3 (UMA) shows a relatively consistent range between 7-10 nm. Consequently, the chemical modifications using ammonia, urea, and magnesium acetate do not significantly impact the change in crystallite size.

The advanced features in catalyst materials pertain to the textural properties that influence the material's capacity in catalytic reactions. The textural properties of all samples, encompassing surface area, average pore diameter, and pore volume, were assessed using N_2-sorption and are presented in Table 3. In Figure 3a, the relationship between the adsorbed gas quantity and relative pressure (P/P_0) is depicted to determine the S_{BET} (Specific Surface Area) of each

Table 2. The 2θ peak values in the XRD patterns for all variants of the γ-Al_2O_3 support.

No	Sample	*hkl*							
		(020)	(120)	(031)	(051)	(151)	(080)	(231)	(512)
1	γ-Al_2O_3-AM1	14.88°	28.50°	38.70°	n.a.	n.a.	n.a.	64.99°	n.a.
2	γ-Al_2O_3-AM2	14.47°	28.14°	38.32°	48.98°	55.19°	n.a.	64.55°	71.94°
3	γ-Al_2O_3-AM3	14.43°	28.11°	38.29°	48.98°	n.a.	n.a.	64.59°	71.94°
4	γ-Al_2O_3-UA1	14.52°	28.19°	38.37°	49.04°	55.21°	60.52°	64.40°	71.94°
5	γ-Al_2O_3-UA2	14.56°	28.27°	38.43°	49.10°	n.a.	n.a.	n.a.	n.a.
6	γ-Al_2O_3-UA3	14.67°	28.41°	38.56°	49.22°	n.a.	n.a.	n.a.	n.a.
7	γ-Al_2O_3-UM1	14.63°	28.31°	n.a.	49.06°	n.a.	60.66°	n.a.	n.a.
8	γ-Al_2O_3-UM2	14.55°	28.22°	38.39°	49.04°	n.a.	60.58°	n.a.	n.a.
9	γ-Al_2O_3-UM3	14.48°	28.14°	38.31°	48.96°	55.17°	60.50°	n.a.	71.88°
10	γ-Al_2O_3-UMA1	14.58°	28.18°	38.34°	48.93°	n.a.	60.59°	n.a.	n.a.
11	γ-Al_2O_3-UMA2	14.60°	28.27°	28.44°	48.93°	n.a.	60.66°	n.a.	n.a.
12	γ-Al_2O_3-UMA3	13.89°	28.40°	38.80°	48.88°	55.48°	61.06°	64.43°	72.13°

Table 3. IR-Py-spectra before and after modification of the HZSM-5 zeolite with boron ([a] determined using N_2-sorption ; [b] determine using the BJH method; [c] determined using the Scherrer equation

No	Sample Code	S_{BET}[a] ($m^2.g^{-1}$)	V_T[a] ($cm^3.g^{-1}$)	d[b] (Å)	D_{cystal}[c] (nm)
1	γ-Al_2O_3-AM1	90.656	0.4597	202.825	8.95
2	γ-Al_2O_3-AM2	138.436	0.7214	208.433	8.00
3	γ-Al_2O_3-AM3	180.918	0.6576	145.394	7.90
4	γ-Al_2O_3-UA1	126.525	1.4280	451.547	9.85
5	γ-Al_2O_3-UA2	147.626	0.6953	188.409	8.32
6	γ-Al_2O_3-UA3	128.411	0.5344	166.458	8.27
7	γ-Al_2O_3-UM1	223.118	0.6881	123.36	7.86
8	γ-Al_2O_3-UM2	170.725	0.7667	179.643	8.69
9	γ-Al_2O_3-UM3	117.113	0.9363	319.779	9.77
10	γ-Al_2O_3-UMA1	243.423	0.6712	132.735	7.96
11	γ-Al_2O_3-UMA2	170.186	0.4489	105.504	9.58
12	γ-Al_2O_3-UMA3	165.074	0.3977	96.376	10.95

sample through linear regression analysis of the graph. Each γ-Al_2O_3 support exhibited a substantial specific surface area of 100-240 m²/g, which could prove advantageous for catalytic applications [25]. The variations in textural properties are attributed to differences in the modification agents used during synthesis. In γ-Al_2O_3 supports modified with ammonia (AM), the resulting S_{BET} is the smallest (90.66 $m^2.g^{-1}$) compared to other modifications. This decrease in surface area may be due to the potential aggregation of particles or partial blockage of pores by residual ammonia species. Meanwhile, supports modified with a combination of urea, magnesium, and ammonia (UMA) exhibit the highest S_{BET} value (243 $m^2.g^{-1}$). This suggests that the presence of magnesium influences the structural arrangement, while urea and ammonia contribute to enhanced porosity by facilitating better dispersion and preventing particle agglomeration.

Pore volume (V_t) also varies across different modifications. The γ-Al_2O_3-UMA-modified catalyst has the smallest pore volume (0.4 $cm^3.g^{-1}$), whereas the γ-Al_2O_3-UA exhibits the largest pore volume (1.4 $cm^3.g^{-1}$). This difference is further reflected in the Barret–Joyner–Halenda (BJH) pore size distribution (Figure 3b), where γ-Al_2O_3-UA has the largest pore size (451 Å), while γ-Al_2O_3-UMA exhibits a smaller pore size

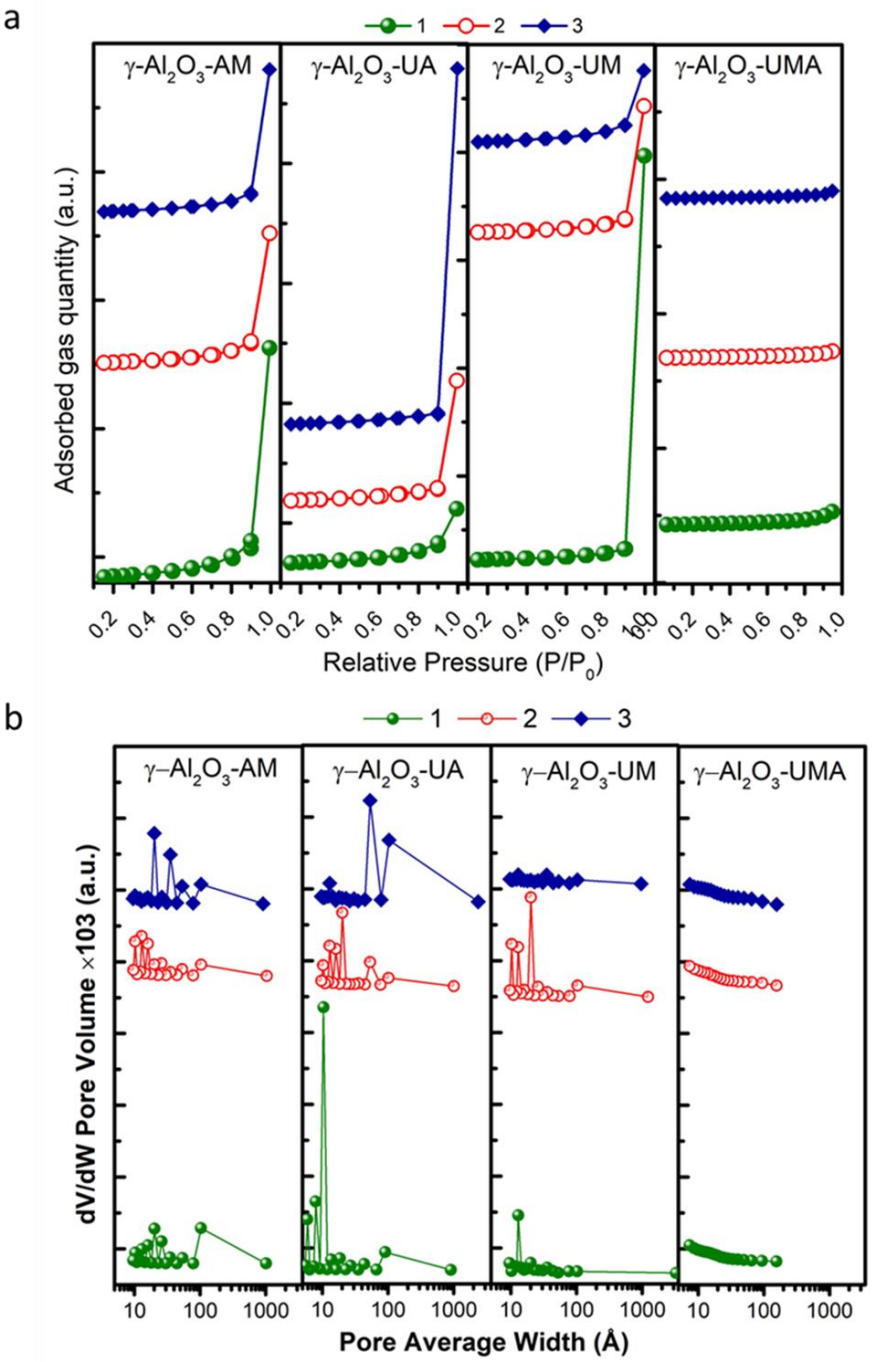

Figure 3. (a) N_2-sorption and (b) BJH pore size distribution of γ-Al_2O_3 support using NH_3 (AM), Urea-NH_3 (UA), Urea-$(CH_3COO)_2Mg$ (UM), and Urea-$(CH_3COO)_2Mg$-NH_3 (UMA) as support variation.

distribution (96 Å). These observations suggest that the use of urea-ammonia (UA) promotes the formation of larger pores, likely due to the role of urea in templating effects or gas evolution during decomposition, which creates a more open structure. In contrast, the UMA modification results in a catalyst with a higher surface area but smaller pore sizes, indicating that the combined effect of urea, magnesium, and ammonia enhances pore wall formation and structural stability [25,26]. These findings highlight the significant impact of modification agents on the surface area, pore volume, and pore size distribution of γ-Al_2O_3 catalysts, which in turn could influence their catalytic performance.

3.2. HDM Catalytic Process

The catalytic performance in the hydrodemetallization (HDM) process was assessed using a model feedstock comprising Fe, V, and Ni-naphthenates dissolved in a paraffinic diesel n-C16-18 solvent. Paraffinic diesel n-C16-18 was chosen as the optimal solvent because of its high solubility for metal naphthenates, superior thermal stability, and physicochemical properties that are comparable to those of petroleum fractions. The identified characteristics create a realistic and stable model system, offering a representative framework for simulating petroleum treatment processes that involve metal contaminants [27,28].

The data in Table 3 indicate that the optimal modification of the γ-Al_2O_3 support, regarding its physical properties—specific surface area, pore volume, and pore size distribution—was attained through treatments with urea in combination with ammonium and with magnesium. The modified supports were impregnated with a NiMo catalyst, yielding two distinct modified catalysts: SM (γ-Al_2O_3 modified with urea and ammonium) and HM (γ-Al_2O_3 modified with urea and magnesium). In catalytic activity testing, an unmodified catalyst, designated as RM, served as a control to assess the performance of the modified catalysts.

Figures 3a, 3b, and 3c depict the HDM process for the removal of Fe, V, and Ni, respectively. The initial concentrations of Fe, Ni, and V in the feedstock were 7.45 ppm, 40 ppm, and 0.63 ppm, respectively. The catalytic activity of the SM, HM, and RM catalysts was systematically assessed over a reaction period of 0 to 120 minutes to evaluate their effectiveness in eliminating metal contaminants. The findings demonstrate that both catalysts possess notable metal removal efficiency, especially during the initial 30 minutes of the reaction. Their performance remains stable over the 120-minute reaction period, indicating durability and sustained catalytic activity under the tested conditions. Figure 3d, 3e and 3f illustrates a comparative analysis of the removal efficiencies of Fe, V, and Ni for both catalysts. The data indicate that SM and HM efficiently remove metal contaminants, achieving an overall removal efficiency of about 85% for the metals tested. The high efficiency demonstrates the effectiveness of these catalysts in lowering metal concentrations in the n- hydrotreated vegetable oil (HVO)

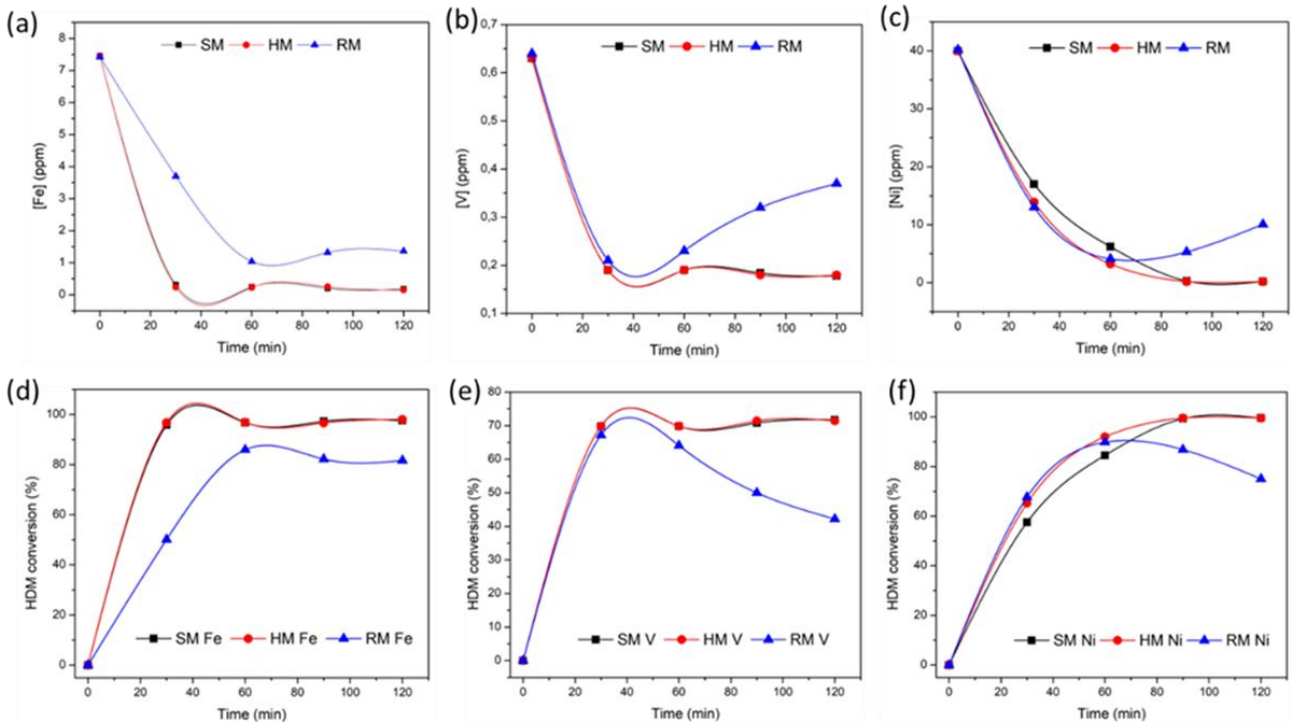

Figure 4. Concentration of (a) Fe, (b) V, and (c) Ni in the hydrodemetallization process utilizing the SM, HM, and RM catalysts, and (d,e,f) percentage HDM conversion.

feedstock, thus improving its purity and quality. The findings support the potential use of HM and SM catalysts in industrial hydrodemetallization, presenting a viable method for enhancing the refining process of metal-containing petroleum feedstocks.

In order to gain a deeper understanding of catalytic hydrodemetallization, we conducted a kinetic evaluation utilizing a set of optimal SM and HM catalysts. Within this investigation, the kinetic parameters were determined to establish the constant rate of this reaction employing pseudo-first-order kinetics [25]. Subsequently, calculations were carried out by creating a graph of ln (C_a/C_{a0}) against time, utilizing the following pseudo-first-order kinetic equation.

$$\frac{dC_a}{dt} = -k \cdot C_r \cdot C_a = -k_{obs} \cdot C_a \quad (1)$$

$$\ln\left(\frac{C_a}{C_{a0}}\right) = -k_{obs} \quad (2)$$

The concentration of the product, denoted as C_a, is a crucial factor in the reaction, alongside the rate constant represented by k. Additionally, the reagent concentration, C_r, is considered and assumed to be zero-order due to it being constantly maintained throughout the reaction. The variable t corresponds to the reaction time. In Figure 4a and Figure 4b, a graphical representation is provided, illustrating the first-order kinetic plot of ln (C_a/C_{a0}) against reaction time (t) and second-order kinetic plot of ($1/C_a$-$1/C_{a0}$) vs. t, respectively, based on previous data on the optimal catalyst [29]. By employing Equation (2), the graph yields a slope that serves as the rate constant (K_{obs}). This observed rate constant (K_{obs}) for each catalyst is subsequently presented in Table 4. Further analysis from the pseudo kinetics order can determine the E_{obs} from the equation as follows:

$$K_{obs} = A\, e^{-\frac{E_{obs}}{RT}} \quad (3)$$

$$\ln K_{obs} = \ln A - \frac{E_{obs}}{RT} \quad (4)$$

where, A represents a pre-exponential factor, and E_{obs} represents the observed activation energy measured in joules per mole (J.mol^{-1}). The universal gas constant, denoted as R, is 8.314 J.mol^{-1}.K^{-1}, and T signifies the temperature in Kelvin (K). To derive the remaining thermodynamic parameters, specifically the enthalpy of activation (ΔH‡) and the entropy of activation (ΔS‡), the Eyring equation (Equation (5)) is employed [30]. Furthermore, the Gibbs free energy of activation (ΔG‡) is determined using Eq. (6). The expressions for these parameters are outlined as follows.

$$\ln\left(\frac{K_{obs}}{T}\right) = \ln\left(\frac{K_B}{h}\right) + \frac{\Delta S^{\ddagger}}{R} - \frac{\Delta H^{\ddagger}}{RT} \quad (5)$$

$$\Delta G^{\ddagger} = \Delta H^{\ddagger} - T \cdot \Delta S^{\ddagger} \quad (6)$$

In heavy oil mixtures containing metals, such as Fe, V, and Ni, these metals are typically bound to the asphaltene structure. Hydrogenation is carried out on intermediate metalloporphyrin compounds within the catalyst pores to remove metals from heavy oil. The result of this reaction will then release metals and sediments that can clog the catalyst pores, reducing its catalytic activity [3,31,32]. This is likely to occur in the reactions conducted in this study, causing the removal process of metals, both Fe and V, to be successful only to the extent of approximately 69-77% of the total metal content present in the feedstock [33–35].

The kinetic rate constant (k_{obs}) presented in Table 4 demonstrates that the SM catalyst (1.20×10^{-2} min^{-1}) shows a higher reaction rate compared to HM (5.85×10^{-3} min^{-1}). This observation implies

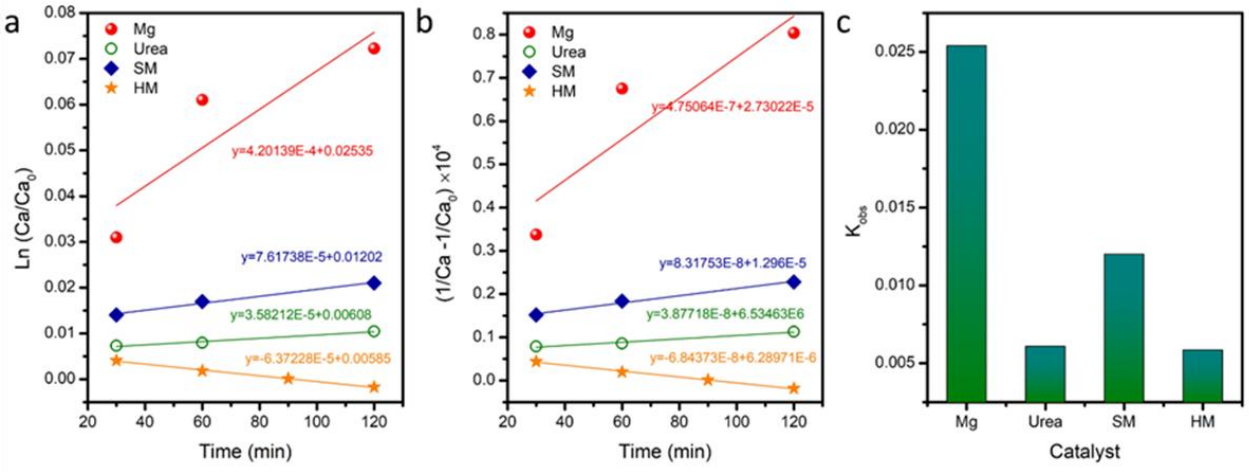

Figure 5. (a) Pseudo first order and (b) second order of n-HVO using HM and SM catalyst in HDM reaction, with (c) the Kobs values for all the tested catalysts in the HDM reaction involving Fe and V in n-HVO were determined.

that the urea-ammonium modification in SM enhances catalytic activity, potentially through increased availability of active sites. Both catalysts demonstrate comparable HDM efficiencies for the removal of Fe, V, and Ni. This suggests that while SM enhances the reaction rate, HM (urea-Mg modification) may play a role in stabilizing the catalyst. In comparison to the Mg-based catalyst (k_{obs} = 2.54 × 10^{-2} min^{-1}), HM exhibits a lower rate constant, suggesting that Mg improves catalytic kinetics. However, the incorporation of urea in HM modifies structural properties, which may influence mass transfer or site accessibility. The findings underscore the trade-off between reaction speed (SM) and catalyst durability (HM), illustrating the unique mechanistic contributions of ammonium and magnesium modifications in enhancing HDM performance.

3.3. HDS Catalytic Process

The catalytic performance in the hydrodesulfurization (HDS) process was evaluated using a standardized paraffinic sulfur compound. The choice of this sulfur standard was intended to create controlled and representative reaction conditions, thereby reducing interference from other compounds that might influence catalytic performance. This method guarantees an accurate and dependable evaluation of the catalyst's desulfurization efficiency. The sulfur concentration was established at 100 ppm to serve as a standard for assessing sulfur removal and catalyst efficacy.

The catalytic activity in the hydrodesulfurization (HDS) process was assessed by examining the performance of SM, HM, and RM catalysts over a reaction duration of 0 to 120 minutes. This study evaluated the effectiveness of each catalyst in the removal of sulfur compounds, while also tracking variations in activity over time. The three catalysts (SM, HM, and RM) effectively reduced the sulfur content of the feedstock in the initial stage of the reaction. After 60 minutes, a decrease in catalytic activity was noted, accompanied by an increase in sulfur concentration.

Figure 6a illustrates that the RM catalyst exhibited the most significant decline in effectiveness, as indicated by a substantial increase in sulfur content following its minimum value. This trend corresponds with the HDS conversion results presented in Figure 6b, demonstrating that the RM catalyst displayed the lowest performance relative to SM and HM. This phenomenon is associated with hydrodemetallization (HDM) activity, indicating that the RM catalyst exhibited reduced efficacy in the removal of heavy metals. The buildup of heavy metals on the catalyst surface and within its pores can obstruct active sites, thereby impeding the HDS reaction and diminishing desulfurization efficiency. The results indicate that the HM catalyst exhibited superior catalytic activity relative to SM and RM, establishing it as the most effective option for desulfurization. The findings underscore the importance of heavy metal removal before hydrodesulfurization (HDS) in optimizing catalyst performance and improving desulfurization efficiency.

Figure 6c illustrates that hydrodesulfurization (HDS) conversion enhances with increasing temperature across all catalysts,

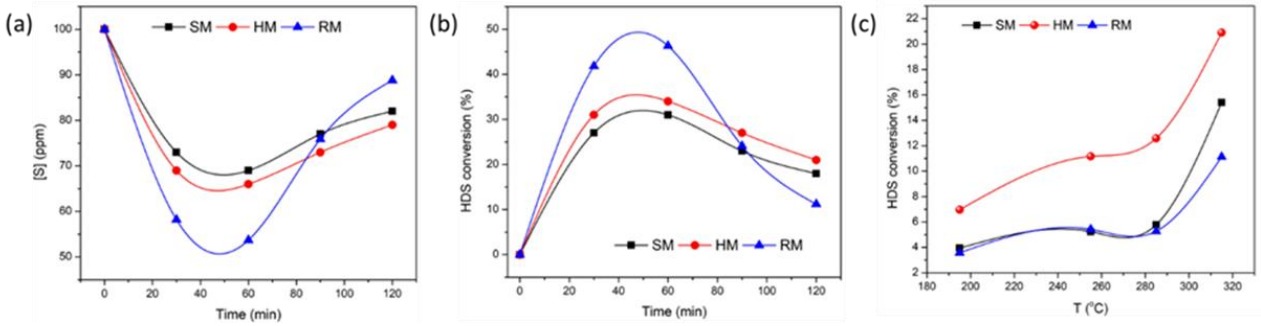

Figure 6. Concentration of (a) S in the hydrodesulfurization process utilizing the SM and HM catalysts, (b) percentage HDS conversion with variation of reaction time, and (c) percentage HDS conversion with reaction temperature variation.

Table 4. Kinetic parameters of catalyst with each modification.

Catalyst	K_{obs} (min^{-1})	%HDM (Fe)	%HDM (V)	%HDM (Ni)
Mg	2.54×10^{-2}	n.a	n.a.	n.a.
Urea	6.08×10^{-3}	n.a	n.a	n.a.
SM	1.20×10^{-2}	97.58	71.75	99.53
HM	5.85×10^{-3}	97.99	71.43	99.53

exhibiting a notable increase beyond 280 °C. The HM catalyst demonstrates superior performance, attaining over 20.9% conversion at 315 °C, with SM following, and RM exhibiting the least effectiveness. The suboptimal performance of RM can be ascribed to pore obstruction caused by heavy metals, which impedes reactant access to active sites. The elevated efficiency of HM indicates that this catalyst possesses more accessible and optimized active sites for the adsorption and conversion of sulfur compounds. Consequently, HM is the preferred catalyst, especially for high-temperature applications aimed at improving desulfurization efficiency.

The effectiveness of catalysts in hydrodesulfurization (HDS) and hydrodemetallization (HDM) is significantly affected by their textural and structural characteristics, especially the pore size. Catalysts with larger pore sizes, such as HM (245 Å), enhance the diffusion of reactants and products and mitigate clogging from heavy metals. Conversely, RM, characterized by the smallest pore size (95 Å), exhibits accelerated clogging, which diminishes its efficacy in heavy metal removal and reduces HDS activity. The data demonstrates a correlation where larger pore sizes are associated with increased HDM and HDS efficiency. HM, characterized by the largest pore size, attains the highest HDS conversion rate at 20.9%. This is followed by SM at 15.4%, whereas RM demonstrates the lowest conversion rate of 11.12%.

The relationship among pore size, HDM efficiency, and HDS efficiency is significantly interconnected. Larger pore catalysts enhance reactant accessibility, optimize active site distribution, and improve resistance to clogging by heavy metals. Thus, HM is identified as the most efficient catalyst in both reactions, whereas SM is a feasible alternative, albeit with slightly reduced effectiveness attributed to its smaller pore size. Conversely, RM demonstrates the lowest effectiveness due to its smaller pore size, which results in accelerated clogging and a marked decrease in both HDM and HDS activity.

The availability and stability of active sites and the textural properties are crucial factors influencing the catalytic efficiency. The accessibility of MoS_2 active sites, essential for hydrodesulfurization (HDS), is impeded by the deposition of heavy metals. Catalysts exhibiting enhanced HDM performance, such as HM and SM, effectively eliminate heavy metals (Fe, V, Ni), thus maintaining a higher quantity of MoS_2 active sites for the HDS reaction. In contrast, RM shows a significant decrease in activity attributed to increased pore clogging and diminished accessibility of active sites. The structural integrity of the catalysts influences their resistance to metal poisoning, with HM exhibiting the highest durability under reaction conditions.

4. Conclusion

The alteration of γ–Al_2O_3 support with ammonia, urea, and magnesium acetate markedly enhanced their structural, textural, and catalytic characteristics for hydrodemetallization (HDM) and hydrodesulfurization (HDS). The modifications affected the catalyst's mineral composition, crystal size distribution, and textural properties, with boehmite crystal sizes consistently ranging from 7 to 10 nm. The modified catalysts treated with urea and ammonia demonstrated increased S_{BET}, V_T, and d values, signifying enhancements in surface area, pore volume, and pore diameter, all of which are essential for catalytic activity. The HM catalyst demonstrated superior efficiency in hydrodesulfurization (HDS) and hydrodemetallization (HDM) reactions, achieving an HDS conversion of 20.9% and HDM efficiencies of 99.52% for Ni, 71.43% for V, and 97.99% for Fe. This advantage is due to its capacity to efficiently eliminate heavy metals, thus preserving the accessibility of active sites. The SM catalyst exhibited HDM performance comparable to HM, achieving efficiencies of 99.52% (Ni), 71.75% (V), and 97.58% (Fe). However, it displayed reduced HDS activity at 15.4%, suggesting a limited number of active sites or inadequate sulfidation. The RM catalyst demonstrated the lowest HDM efficiency, recording 74.99% for Ni, 42.19% for V, and 81.67% for Fe, alongside an HDS conversion of merely 11.12%. This underscores the constraints in both the quantity and efficacy of active sites, attributed to accelerated pore blockage. The catalyst's pore size significantly influences the efficiency of hydrodesulfurization (HDS) and hydrodeoxygenation (HDM). HM, with the largest pore size of 245 Å, exhibits the highest activity, while SM at 205 Å and RM at 95 Å demonstrate more rapid pore blockage. Consequently, HM serves as the most effective catalyst for desulfurization applications, with SM following, and RM demonstrating the least efficacy in both reactions. Pore size is the primary factor influencing HDM and HDS activity, with surface area and pore volume following in importance. HM is identified as the most effective catalyst, followed by SM, whereas RM demonstrates the least performance attributed to rapid pore blockage and diminished active site availability. The findings highlight the significance of textural properties in the design of catalysts for effective hydrodesulfurization and hydrodemetallization processes.

Acknowledgement

The authors wish to thank to PT Pertamina Technology & Innovation (TI) for providing the research fund.

CRediT Author Statement

Author Contributions: W. Rustyawan contributed to conceptualization, methodology, investigation, resources, data curation, writing, and manuscript review and editing. I.G.B.N. Makertihartha, C.B. Rasrendra, and O. Muraza supervised the study, provided methodological input, and contributed to manuscript revision. G.T.M. Kadja and N. Nurdini wrote the initial draft of the manuscript. I. Gamar provided feedback on the manuscript. All authors have read and approved the final version of the manuscript.

References

[1] Chehadeh, D., Ma, X., Bazzaz, H. Al (2023). Recent progress in hydrotreating kinetics and modeling of heavy oil and residue : A review. *Fuel*, 334(P1), 126404. DOI: 10.1016/j.fuel.2022.126404.

[2] Ferreira, C., Guibard, I., Lemos, F. (2014). Hydrodesulfurization and hydrodemetallization of different origin vacuum residues : New modeling approach. *Fuel*. 129, 267–277. DOI: 10.1016/j.fuel.2014.03.056

[3] Nguyen, T., Nguyen, Q., Ngoc, A., Cao, T., Ernest, T., Binh, T., Pham, P.T.H., Nguyen, T.M. (2022). Journal of Petroleum Science and Engineering Hydrodemetallization of heavy oil : Recent progress, challenge, and future prospects AR. *Journal of Petroleum Science and Engineering*, 216(January), 110762. DOI: 10.1016/j.petrol.2022.110762.

[4] Gab, M.A., Adel, A. (2021). Determination of iron, nickel, and vanadium in crude oil by inductively coupled plasma optical emission spectrometry following microwave - assisted wet digestion. *Chemical Papers*, 75, 4239–4248. DOI: 10.1007/s11696-021-01633-8

[5] Pereira, J.S.F., Moraes, D.P., Antes, F.G., Diehl, L.O., Santos, M.F.P., Guimarães, R.C.L., Fonseca, T.C.O., Dressler, V.L., Flores, É.M.M. (2010). Determination of metals and metalloids in light and heavy crude oil by ICP-MS after digestion by microwave-induced combustion. *Microchemical Journal*, 96(1), 4–11. DOI: 10.1016/j.microc.2009.12.016.

[6] Hensen, E.J.M., Poduval, D.G., Veen, J.A.R. Van (2007). Promotion of Thiophene Hydrodesulfurization by Ammonia over Amorphous-Silica - Alumina-Supported CoMo and NiMo Sulfides. *Industrial & Engineering Chemistry Research*, 46(12), 4202–4211. DOI: 10.1021/ie0611756

[7] Kim, J.H., Jung, K.Y., Park, K.Y. (2012). Journal of Industrial and Engineering Chemistry Effect of urea, NH4OH, and DCCA on texture properties of alumina prepared by ultrasonic spray pyrolysis. *Journal of Industrial and Engineering Chemistry*, 18(1), 344–348. DOI: 10.1016/j.jiec.2011.04.001.

[8] Hamid Al-megren, Y.H., Haoyi Chen, Mohammed Alkinany Sergio Gonzalez-Cortes, Saud Aldrees, T.X. (2015). Effect of urea / metal ratio on the performance of NiMoP/Al2O3 catalyst for diesel deep HDS. *Applied Petrochemical Research*, 5, 173–180. DOI: 10.1007/s13203-015-0098-x

[9] Chen, L., Xu, Y., Wang, B., Yun, J., Dehghani, F., Xie, Y. (2021). Mg-modified CoMo/Al2O3 with enhanced catalytic activity for the hydrodesulfurization of 4,6-dimethyldibenzothiophene. *Catalysis Communications*, 155, 106316. DOI: 10.1016/j.catcom.2021.106316.

[10] Chen, W., Nie, H., Li, D., Long, X., Gestel, J. Van, Maugé, F. (2016). Effect of Mg addition on the structure and performance of sulfide Mo / Al 2 O 3 in HDS and HDN reaction. *Journal of Catalysis*, 344, 420–433. DOI: 10.1016/j.jcat.2016.08.025.

[11] Liu, T., Ju, L., Zhou, Y., Wei, Q., Ding, S., Zhou, W., Luo, X., Jiang, S., Tao, X. (2015). Effect of pore size distribution (PSD) of Ni-Mo/Al2O3 catalysts on the Saudi Arabia vacuum residuum hydrodemetallization (HDM). *Catalysis Today*, 3–11, 271, 179–187. DOI: 10.1016/j.cattod.2015.07.045.

[12] Zhu, H., Mao, Z., Liu, B., Yang, T., Feng, X., Jin, H., Peng, C., Yang, C., Wang, J., Fang, X. (2020). Regulating catalyst morphology to boost the stability of Ni-Mo/Al2O3 catalyst for ebullated-bed residue hydrotreating. *Green Energy and Environment*, 6(2), 283–290. DOI: 10.1016/j.gee.2020.05.001

[13] Marques, J., Guillaume, D., Merdrignac, I., Espinat, D., Brunet, S. (2011). Applied Catalysis B : Environmental Effect of catalysts acidity on residues hydrotreatment. *Applied Catalysis B : Environmental*, 101(3–4), 727–737. DOI: 10.1016/j.apcatb.2010.11.015.

[14] Ramli, Z., Saleh, R. (2008). Preparation of Ordered Mesoporous Alumina Particles via Simple Precipitation Method. *Journal of Fundamental Sciences*, 4(2), 435–443. DOI: 10.11113/mjfas.v4n2.52

[15] Qin, H., Tan, X., Huang, W., Jiang, J., Jiang, H. (2015). Application of urea precipitation method in preparation of advanced ceramic powders. *Ceramics International*, 41(9), 11598–11604 DOI: 10.1016/j.ceramint.2015.06.032.

[16] Ameri, E., Abdollahifar, M., Zamani, M. R., Nekouei, H. (2016). The Role of Urea on The Hydrothermal Synthesis of Boehmite Nanoarchitectures. *Ceramics-Silikaty*, 60(3), 162–168. DOI: 10.13168/cs.2016.0025.

[17] Yang, J., Frost, R.L. (2008). Synthesis and Characterization of Boehmite Nanofibers. 2008(25 mL). *Research Letters in Inorganic Chemistry*, 2008(1), 1–4. DOI: 10.1155/2008/602198.

[18] Souza, P. De, Carlos, A., Coelho, V., São, U. De, Usp, P., Prof, A., Gualberto, L., Sp, S.P., Sp, S.P. (2009). Hydrothermal Synthesis of Well-Crystallised Boehmite Crystals of Various Shapes. *Materials Research*, 12(4), 437–445. DOI: 10.1590/S1516-14392009000400012.

[19] Stuart, N.M., Sohlberg, K. (2021). The Microstructure of γ-Alumina. 1–16. *Energies,* 14(20), 1–16. DOI: 10.3390/en14206472.

[20] Javad, M., Mehdi, F., Davood, E. (2017). Performance enhancement of quantum dot sensitized solar cells by treatment of ZnO nanorods by magnesium acetate. *Journal of Materials Science: Materials in Electronics*, 29, 4569–4574. DOI: 10.1007/s10854-017-8407-z.

[21] Polu, A.R., Kumar, R. (2013). Ionic Conductivity and Discharge Characteristic Studies of PVA-Mg (CH3COO)2 Solid Polymer Electrolytes. *International Journal of Polymeric Materials and Polymeric Biomaterials*, 62(2), 76–80. DOI: 10.1080/00914037.2012.664211.

[22] Nasiri, S., Rabiei, M., Palevicius, A., Janusas, G., Vilkauskas, A., Nutalapati, V., Monshi, A. (2023). Nano Trends Modified Scherrer equation to calculate crystal size by XRD with high accuracy , examples Fe2O3, TiO2 and V2O5. *Nano Trends*, 3(August), 100015. DOI: 10.1016/j.nwnano.2023.100015.

[23] Nurdini, N., Mualliful, M., Maryanti, E., Setiawan, P., Thomryes, G., Kadja, M. (2022). Heliyon Thermally-induced color transformation of hematite : insight into the prehistoric natural pigment preparation. *Heliyon*, 8(8), e10377. DOI: 10.1016/j.heliyon.2022.e10377.

[24] Gunawan, M.L., Muntaqin, A., Saraswati, M.A., Nurdini, N., Kadja, G.T.M., Rasrendra, C.B. (2024). Case Studies in Chemical and Environmental Engineering Supreme efficacy : The ultrahigh performance of ZnO adsorbent for ambient-temperature H2S removal in integrated H2S – N2 gas. *Case Studies in Chemical and Environmental Engineering*, 9(10), 100615. DOI: 10.1016/j.cscee.2024.100615.

[25] Rasrendra, C.B., Maulidanti, E.G., Darlismawantyani, S.E.P., Nurdini, N., Rustyawan, W., Kadja, G.T.M. (2023). Case Studies in Chemical and Environmental Engineering Bifunctional NiMo / HY-γ-Al2O3 catalysts for an effective production of ultra-low sulfur diesel. *Case Studies in Chemical and Environmental Engineering*, 8(May), 100427. DOI: 10.1016/j.cscee.2023.100427.

[26] Goede, S. De, Wilken, C., Ajam, M., Roets, P., Engelbrecht, P., Woolard, C. (2015). A Comparison of the Stability Performance of Blends of Paraffinic Diesel and Petroleum-Derived Diesel , with RME Biodiesel Using Laboratory Stability Measurement Techniques. *Journal of Fuels*, 2015, 528497. DOI: 10.1155/2015/528497.

[27] Alatrsh, S., Ilter, S. (2022). Performance Review of C18 Paraffin Phase Changing Building Materials in Different Climate Zones. *International Journal of Civil Engineering*, 9(8), 22–28. DOI: 10.14445/23488352/IJCE-V9I8P104

[28] Chang, J., Liu, J., Li, D. (1998). Kinetics of resid hydrotreating reactions. *Catalysis Today*, 43(3–4), 233–239. DOI: 10.1016/S0920-5861(98)00152-7.

[29] Erika, D., Nurdini, N., Mulyani, I., Kadja, G.T.M. (2023). Amine-functionalized ZSM-5-supported gold nanoparticles as a highly efficient catalyst for the reduction of p-Nitrophenol. *Inorganic Chemistry Communications*, 147(10), 110253. DOI: 10.1016/j.inoche.2022.110253.

[30] Pal, N., Verma, V., Khan, A., Mishra, A., Anand, M. (2022). Hydrotreating and hydrodemetalation of raw jatropha oil using mesoporous Ni-Mo/γ-Al2O3 catalyst. *Fuel,* 326, 125108. DOI: 10.1016/j.fuel.2022.125108.

[31] Ghassabzaadeh, H., Niaei, A., Rashidzadeh, M. (2020). Synthesis and Characterization of Multi-Modal γ-Al2O3 : A Systematic Investigation on the Optimization of Hydrodemetallization Catalyst Preparation. *Chemistry Select*, 5(29), 8892–8905. DOI: 10.1002/slct.202001252.

[32] Garcia-montoto, V., Verdierc, S., Maroun, Z., Egeberg, R., Tiedje, J.L. (2020). Understanding the removal of V, Ni and S in crude oil atmospheric residue hydrodemetallization and hydrodesulfurization. *Fuel Processing Technology*, 201, 106341. DOI: 10.1016/j.fuproc.2020.106341.

[33] Li, G., Lu, X., Tang, Z., Liu, Y., Li, X., Liu, C. (2013). Preparation of NiMo/g -Al2O3 catalysts with large pore size for vacuum residue hydrotreatment. *Materials Research Bulletin*, 48(11), 4526–4530. DOI: 10.1016/j.materresbull.2013.07.041.

[34] Gualda, G. (1996). Initial Deactivation of Residue Hydrodemetallization Catalysts. *Journal of Catalysis*, 161(1), 319–337. DOI: 10.1006/jcat.1996.0190.